Research Article

Bioactivity behavior of Ag_2O or CuO doped in glass systems of $Na_2O–CaF_2–P_2O_5$ and $Na_2O–CaO–P_2O_5$ and their glass–ceramic derivatives assessed by FTIR, X-ray diffraction and SEM measurements

A. M. Fayad[1] · M. A. Marzouk[1] · F. H. El-Batal[1]

Abstract
Glasses from the two systems ($Na_2O–CaF_2–P_2O_5$) and ($Na_2O–CaO–P_2O_5$) doped with 0.2% CuO or Ag_2O were prepared by melting annealing technique. Samples from the glasses were thermally heat treated to convert them to their glass–ceramic derivatives. FTIR spectra of the glasses and glass–ceramics were examined before and after immersion in SBF for 2 weeks at 37 °C to justify the spectral changes correlated with the bioactivity behavior of the tested samples. X-ray diffraction was utilized to identify the formed crystalline phases in the glass–ceramics upon thermal heat treatment. The crystalline phases are identified to be dependent on the chemical composition of the base glass and consisting of sodium phosphate and calcium phosphate crystalline phases beside combined sodium calcium fluoride phosphate crystalline phases and the sharing of the dopants. FTIR spectra after immersion indicate the appearance of two far-IR peaks which are characteristic for calcium phosphate or hydroxyapatite. SEM investigations confirm the bioactivity behavior through the appearance of the rounded or nodular-shaped crystalline phase. The optical and PL spectra indicate the complete transparency of the glasses in the visible except of interference of UV absorption band due to trace ferric ions impurities.

Keywords Phosphate glass · Glass–ceramic · Invitro bioactivity · FTIR · PL spectra · Optical

1 Introduction

Phosphate glasses belong to a special vitreous system which are composed of connected tetrahedral PO_4 units containing a single double bond with oxygen (P=O) to compensate for the pentavalent phosphorous atom [1]. They possess extended chemical compositions and retaining always the tetrahedral PO_4 units beside the low preparation temperatures and hence low transition temperatures which make some of them to be suitable candidate as solder glass and sealing purposes [2, 3]. Their excellent optical properties with many of the divalent metal oxides (MgO, ZnO, PbO, SrO, BaO, CaO) or with the addition of fluorides to obtain fluorophosphate glasses combining both properties of oxides and fluorides as evidenced by Ehrt and Möncke [4, 5]. The authors have reached the conclusion about the applications of phosphate and fluorophosphates glasses in special recent optical devices. Phosphate glasses combined with PbO and Fe_2O_3 are suitable candidates for encapsulation of some radioactive wastes because of their superior chemical durability than borosilicate glasses and can conduct shielding behavior toward many irradiations [6].

Phosphate glasses have also great potential as regenerative medicine because of their solubility as strongly composition-dependent beside their bioactivity behavior [7–10]. However, some authors [11] have revealed that the beneficial range of phosphate glasses for biomedical applications is bounded not only because of crystallization effects, but in vitro studies have displayed that too high solubility is detrimental to cell activity [8].

✉ F. H. El-Batal, fh_elbatal@yahoo.co.uk | [1]Glass Research Department, National Research Centre, 33 EL Bohouth St. (Former EL Tahrir St.), Dokki, P. O. 12622, Giza, Egypt.

SN Applied Sciences (2019) 1:203 | https://doi.org/10.1007/s42452-019-0215-z

Received: 11 October 2018 / Accepted: 24 January 2019 / Published online: 2 February 2019

Phosphate glasses can incorporate relatively high percent of 3*d* transition metal ions, rare-earth ions and noble metals and exhibit interesting optical, magnetic and electrical properties [12–14]. Some of the phosphate glasses containing ZnO or MgO reveal anomalous behavior in some of their properties and such behavior is related to the change in the coordination number of Mg^{2+} or Zn^{2+} [15]. Marzouk et al. [16] have shown that binary zinc phosphate glass shows anomalous behavior in both thermal expansion property and crystallization behavior, while binary barium phosphate glass exhibits normal response.

The main target of the present work is to characterize and compare bioactivity behavior of glasses from the two systems Na_2O–CaF_2–P_2O_5 or Na_2O–CaO–P_2O_5 containing dopants of (0.2% CuO) or (0.2% Ag_2O). The work includes the measurements of photoluminescence and FT infrared spectra of the glasses and their corresponding glass–ceramic derivatives. Further studies have been directed to investigate X-ray diffraction patterns and scanning electron microscopic images of the prepared glass–ceramics to identify the formed crystalline phases and their morphological textures and their variation after immersion in SBF for 2 weeks at 37 °C.

Some authors have investigated the bioactivity behavior of Na_2O–CaO–P_2O_5 glasses with and without dopants [17–19]. The results showed that the addition of 0.5 TiO_2 enhanced the bioactivity to a measurable extent in vivo study [18], and the addition of Ag_2O to this glass demonstrates an antibacterial effects [19].

2 Experimental details

2.1 Preparation of the glasses

The glasses were prepared from common purity grade chemicals including ammonium dihydrogen orthophosphate ($NH_4H_2PO_4$), calcium carbonate ($CaCO_3$), calcium fluoride (CaF_2), sodium carbonate (Na_2CO_3) and the dopants as CuO, $AgNO_3$ (for Ag_2O).

The accurately weighed batches listed in Table 1 (50 g total) were melted in covered porcelain crucibles at 1100 °C ± 100 °C for 60 min in SiC-heated furnace (Vecstar, UK). The melts were rotated every 20 min to reach complete mixing and homogeneity. The homogenized melts were poured into warmed stainless steel molds with the dimensions required. The prepared glassy samples were transferred immediately to an annealing muffle regulated at 280 °C. The muffle was switched off after 1 h with the glasses inside and left to cool to room temperature at a rate of 30 °C/h.

For optical and PL measurements, samples with the dimensions (4 cm × 1 cm × 0.2) were prepared and for other measurements different sizes and powdered samples were prepared by careful grinding in agate mortar for IR disk technique.

2.2 Preparation of the corresponding glass–ceramics

The parent glasses were subjected to controlled heat treatment process with two-step regime. The glasses were first heated in a muffle furnace with a rate of 5 °C/min to reach 300 °C and kept at this temperature for 12 h and then, the temperature of the muffle was raised to reach 380 °C and kept at this second temperature for 6 h. The muffle was then switched off and then left to cool to room temperature at a rate of 30 °C/h.

2.3 Bioactivity measurements

In order to estimate the in vitro bioactivity test of the glass and glass–ceramic specimens, we used the SBF as proposed by Kokubo et al. [20]. The Tris-buffered SBF composition is (Na^+142.0, K^+5.0, Mg^{2+}1.5, Ca^{2+}2.5, Cl^-147.8, HCO_3^-5.0, HPO_4^{2-}1.0 and SO_4^{2-}0.5 mol m^{-3}). The specimens were vertically mounted on a nylon wire in polyethylene falcon test tubes containing 50 ml of SBF for 14 days at 37 ± 0.5 °C and pH = 7.2 ± 0.3, using HCl 0.1 N for pH adjustment. After the immersion time (2 weeks), the samples were gently rinsed with deionized water and acetone and dried in air at room temperature.

Table 1 Chemical composition of the prepared glasses

Sample	P_2O_5	Na_2O	CaF_2	CaO	Ag_2O	CuO
1	61	27	12	–	–	–
2	61	27	12	–	0.2	–
3	61	27	12	–	–	0.2
4	61	27	–	12	–	–
5	61	27	–	12	0.2	–
6	61	27	–	12	–	0.2

2.4 X-ray diffraction analysis

The identification of the crystalline phases formed during controlled thermal heat treatment and formation of glass–ceramics was carried out by a diffractometer (Bruker Axs-CD8 Advance) with Cu–Ka radiation operating at 40 kV and 10 mA. The diffraction data collected for 2θ values between 10° and 70°, and the scanning speed was 2°/min.

2.5 Fourier transform infrared absorption measurements

FTIR absorption spectra of the glasses and glass–ceramics were measured at room temperature in the wavenumber range 400–4000 cm^{-1}, with a resolution of 2 cm^{-1} by FTIR spectrometer type (JASCO, 4600, Japan) using the KBr disk technique. Pulverized glass or glass–ceramic was mixed in a 1:1000 wt ratio with spectroscopic KBr. The mixture was then subjected to 5t cm^{-2} load in an evocable die to produce homogeneous clear disks. At least, two spectra for each sample were recorded. The spectrum of each sample was taken as the average of 30 scans, FTIR spectra were corrected for the dark current noises and background using the two point baseline. The measurements were carried immediately to avoid moisture water attack to the powders.

2.6 Scanning electron microscopic investigations

SEM measurements of the surfaces of glass–ceramics were carried out using an SEM apparatus model (Philips XL, 30) operating with accelerating voltage 30 kV. All glass–ceramic samples were coated with surface layer of Au for morphological studies.

2.7 Optical absorption measurements

Optical (UV–visible) absorption measurements were carried out on equal thickness polished samples (2 mm ± 0.1 mm) using a recording spectrophotometer (type T 80 t, PG Instrument Ltd, England) covering the range from 200 to 1100 nm.

2.8 Photoluminescence measurements

Photoluminescence measurements for the glasses and glass–ceramics were recorded at room temperature under the excitation wavelength of 266 nm for Ag_2O, 380 nm for CuO in the spectral range 300–700 nm using a fluorescence spectrophotometer type JASCO, FP-6500, Japan) equipped with a xenon flash lamp as the excitation light source. The scan speed is 0.15 step-1 with a step length of 0.2 nm and slit width 0.2 nm.

3 Results

3.1 X-ray diffraction patterns of the glass–ceramic derivatives

Figure 1 depicts the XRD patterns data of the glass–ceramics of the undoped and CuO- or Ag_2O-doped glass–ceramics from the system Na_2O–CaF_2–P_2O_5. The detailed identified crystalline phases are summarized as follows:

1. The undoped glass–ceramic shows four crystalline phosphate phases with the main phase of calcium phosphate ($Ca_3(PO_4)_2$) with (32.3%) and with two sodium phosphates: the sodium phosphate hydrate $Na_3PO_4(H_2O)_8$ with (50.5%), sodium phosphate $(NaPO_3)_6$ with (14.2%) and sodium calcium fluoride phosphate $Na_2Ca_4(PO_4)_3F$ with (3%).
2. The CuO-doped glass–ceramic reveals the same four crystalline phosphate phases as the undoped glass–ceramic with the increase in the percent of calcium phosphate than the percent of the two sodium phosphates beside the mixed sodium calcium fluoride phosphate crystalline phase.
3. The Ag_2O-doped glass–ceramic shows also the same four crystalline phosphates similar to the phases of the undoped glass–ceramic with the appearance of (Ag) ions beside the mixed sodium calcium fluoride phosphate crystalline phase.

Figure 2 reveals the XRD of the glass–ceramics of the undoped and CuO-or Ag_2O-doped glass–ceramics from the system Na_2O–CaO–P_2O_5.

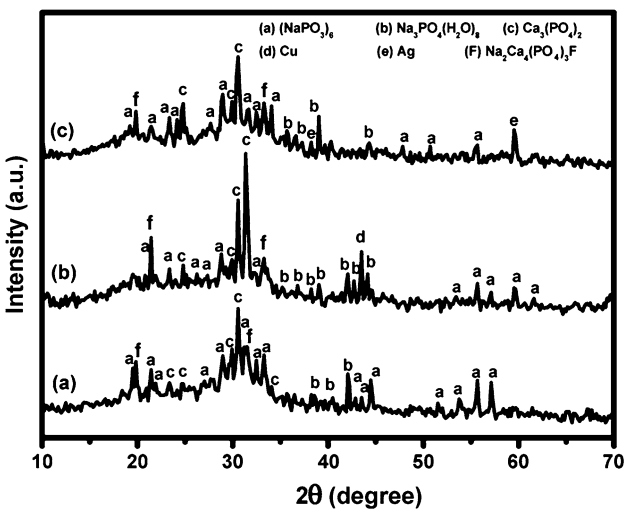

Fig. 1 XRD of sodium calcium fluorophosphates glass–ceramics (a) undoped (b) CuO and (c) Ag_2O

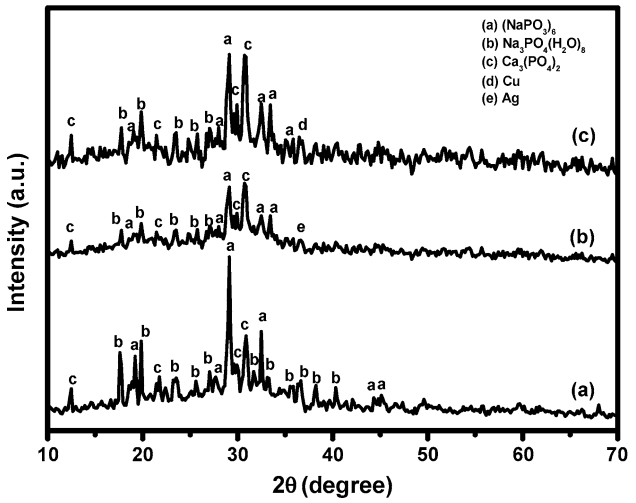

Fig. 2 XRD of sodium calcium phosphates glass–ceramics (a) undoped (b) CuO and (c) Ag_2O

The detailed identified crystalline phases are summarized as follows:

(1) The undoped glass–ceramic shows the main crystalline phases consisting main sodium phosphate with secondary phase of sodium phosphate hydrate, while the calcium phosphate crystalline phase is the lowest percent.
(2) The two doped glass–ceramics reveal the appearance of sodium phosphate and calcium phosphate crystalline phases as two main phases, and the third sodium phosphate hydrate phase is the lowest percent beside the appearance of crystalline species of Ag or Cu.

3.2 FT infrared absorption spectra of the glasses and glass ceramics before and after immersion

3.2.1 FTIR spectra of the group ($NaO–CaF_2–P_2O_5$) glasses and glass–ceramics

Figure 3a, b illustrates the FTIR spectra of the $Na_2O–CaF_2–P_2O_5$ glasses and glass–ceramics. The IR vibrational spectral bands of the glasses are identified to be concentrated within the mid region (400–1650) cm^{-1} for all the samples.

The IR spectrum of the undoped glass reveals the following spectral details:

(a) The far-IR region shows four peaks at 402, 548, 711, 740 cm^{-1}.
(b) A very broad band extending from 850 to 1650 cm^{-1} with seven connected peaks at 880, 1026, 1134, 1270, 1390, 1457 and 1637 cm^{-1}.

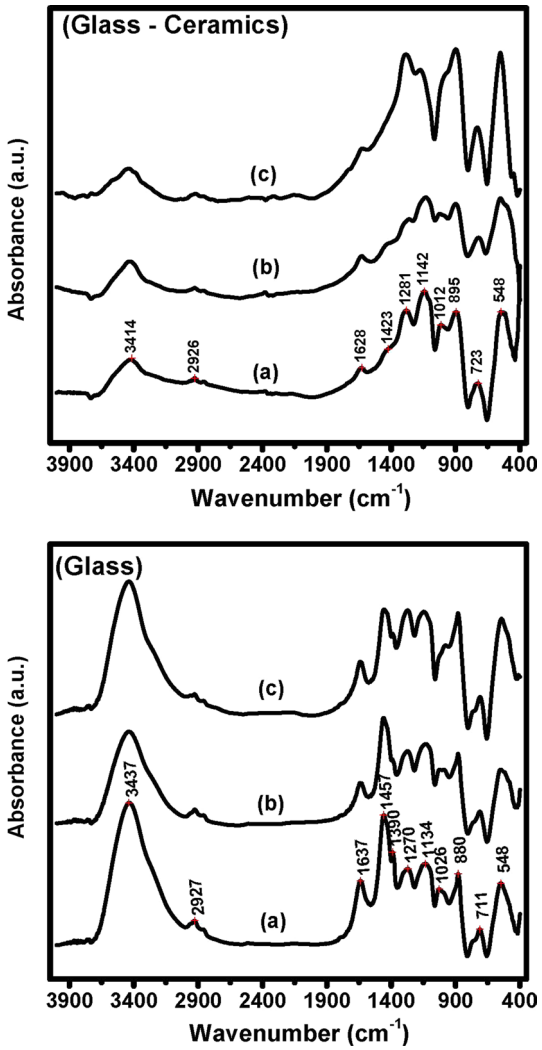

Fig. 3 FTIR absorption spectra of sodium fluorophosphates glass and their inverted glass ceramics before immersion (a) undoped (b) Ag_2O and (c) CuO

(c) The near-IR region shows two small peaks at 2840, 2927 and followed by a broad and high intense band centered at 3437 cm^{-1}.

The IR spectra of the two doped glasses reveal almost repetitive spectral vibrational bands, but the intensity of the peak at 1450 cm^{-1} decreases and becomes similar to the previous neighboring peaks at 1134 and 1270 cm^{-1}.

The IR spectra of the glass–ceramic samples from the same system reveal almost the same vibrational bands as that for the parent glasses. But, the most important difference between the two spectra is the distinct decrease in the intensities of the peaks at 1450, 1640 cm^{-1} and the near-IR broad band around 3437 cm^{-1}.

3.2.2 FTIR spectra of the glasses and glass–ceramics from the glass system Na_2O–CaO–P_2O_5

Figure 4 illustrates the FTIR spectra of the glasses and glass–ceramics from the system soda lime phosphate before immersion.

The IR spectrum of the undoped glass reveals condensed vibrational peaks within the mid range 400–1650 cm^{-1} and with a small peak at 2924 cm^{-1} and a broad band in the near-IR region centered at 3432 cm^{-1}. The detailed vibrational bands of the undoped glass (4a) are summarized as follows:

(a) A distinct and sharp far-IR band is recognized at 513 cm^{-1}.

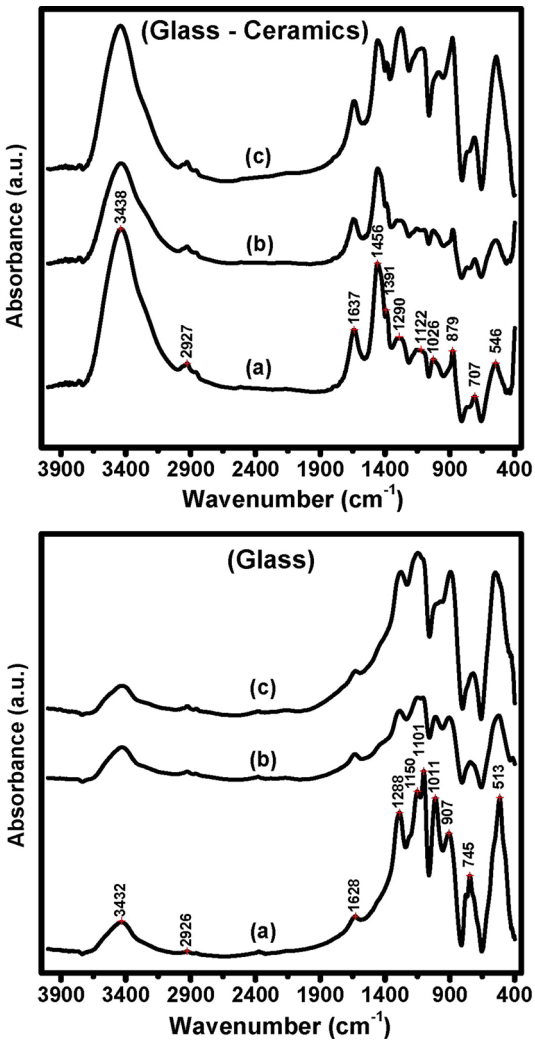

Fig. 4 FTIR absorption spectra of sodium calcium phosphate glass and their inverted glass ceramics before immersion (a) undoped (b) Ag_2O and (c) CuO

(b) A medium two-split band is observed with peaks at 745 and 765 cm^{-1}.
(c) A composite connected band is identified to be extended from about 850 to 1400 cm^{-1} with five distinct peaks at 907, 1011, 1101, 1150 and 1288 cm^{-1}.
(d) A separate small peak is identified at 1628 cm^{-1}.
(e) A very small peak is observed within the near-IR region at 2926 cm^{-1} followed by a broad mid band centered at 3432 cm^{-1}.

The two other doped glasses show nearly the same vibrational peaks, but reveal some differences in the intensities of the peaks in the region 900–1200 cm^{-1}.

The IR spectra of the glass–ceramic samples also reveal condensed IR peaks within the region from 400 to 1600 cm^{-1}, but with distinct variations in the intensities of the mid region peaks with the change in the dopant oxide. The most characteristic feature of the IR spectra of the glass–ceramic samples is the distinctive appearance with high intensity of the bands at about 1460, 1640 and 3430 cm^{-1}.

3.2.3 FTIR spectra of the glasses and glass–ceramics after immersion

The IR spectra of the group (1) after immersion appear (Fig. 5) concentrated or composite in the mid region (400–1600 cm^{-1}) as before immersion but with few variations from that before immersion (Fig. 3) which are summarized as follows:

1. The far-IR bands at about 520–550 and 715–728 cm^{-1} remain distinct without any changes.
2. The mid peaks at about 890 and 980 cm^{-1} remain almost unchanged.
3. The mid peaks at about 1130 and 1265 cm^{-1} increase in their intensities in the glasses, but the first peak is highly increased in the two doped glass–ceramic samples.
4. The peak at 1450 cm^{-1} is almost disappeared.
5. The peak at about 1540 cm^{-1} decreases in intensity in the glasses and glass–ceramics.
6. The near-IR broad band highly decreases in intensity in all the glasses, but slightly decreases in the glass–ceramic samples.

The IR spectra of the group (2) glasses or glass–ceramics after immersion (Fig. 6) appear also composite as before immersion (Fig. 4) and the identified changes are summarized as follows:

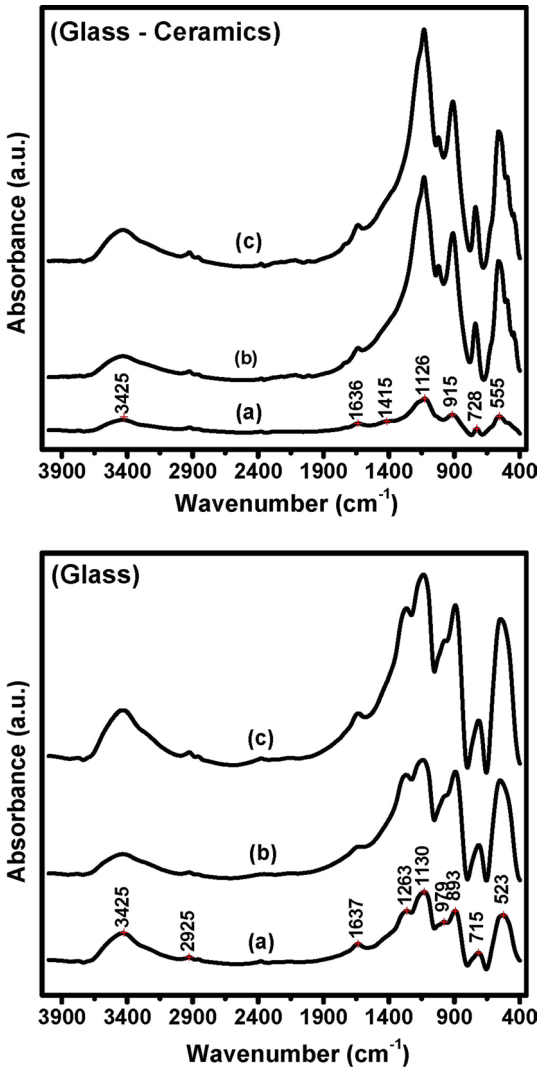

Fig. 5 FTIR absorption spectra of sodium calcium fluorophosphates glass and their inverted glass ceramics after immersion (a) undoped (b) Ag_2O and (c) CuO

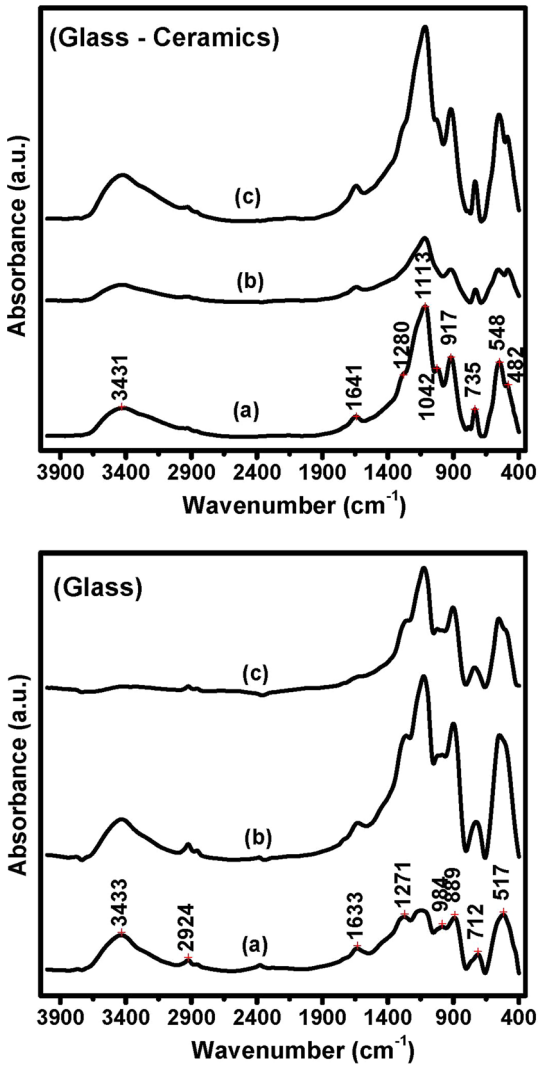

Fig. 6 FTIR absorption spectra of sodium calcium phosphates glass and their inverted glass ceramics after immersion (a) undoped (b) Ag_2O and (c) CuO

1. The intensities of all the vibrational bands of the glasses are generally observed to decrease with immersion.
2. The far-IR bands at about 517 and 712 cm^{-1} remain almost distinct with very small decrease in intensity.
3. The bands at about 1130 and 1270 cm^{-1} are mostly remain persistent or distinct after immersion.

3.3 Scanning electron microscopic investigations

Figure 7 illustrates the SEM images of the glass–ceramics of group (1) (Na_2O–CaF_2–P_2O_5) before and after immersion. The various morphological features identified are summarized as follows:

1. The electron micrographs of the glass ceramics before immersion reveal different images including different shaped microcrystalline features for the undoped, Cu-doped and Ag_2O-doped samples. On the other hand, the images after immersion show in all glass ceramics rounded or nodular-shaped microcrystals, but somewhat different in their arrangements or intensity.
2. Before immersion, the undoped glass–ceramic shows acicular-shaped microcrystals within fine grained matrix. The CuO-doped glass–ceramic reveals mostly uniform grained texture. The Ag_2O-doped glass–ceramic shows mostly gathering of microcrystalline features of nodular shape with parts of uniform texture.
3. The glass–ceramic samples after immersion exhibit nodular-shaped microcrystals of moderate extent in

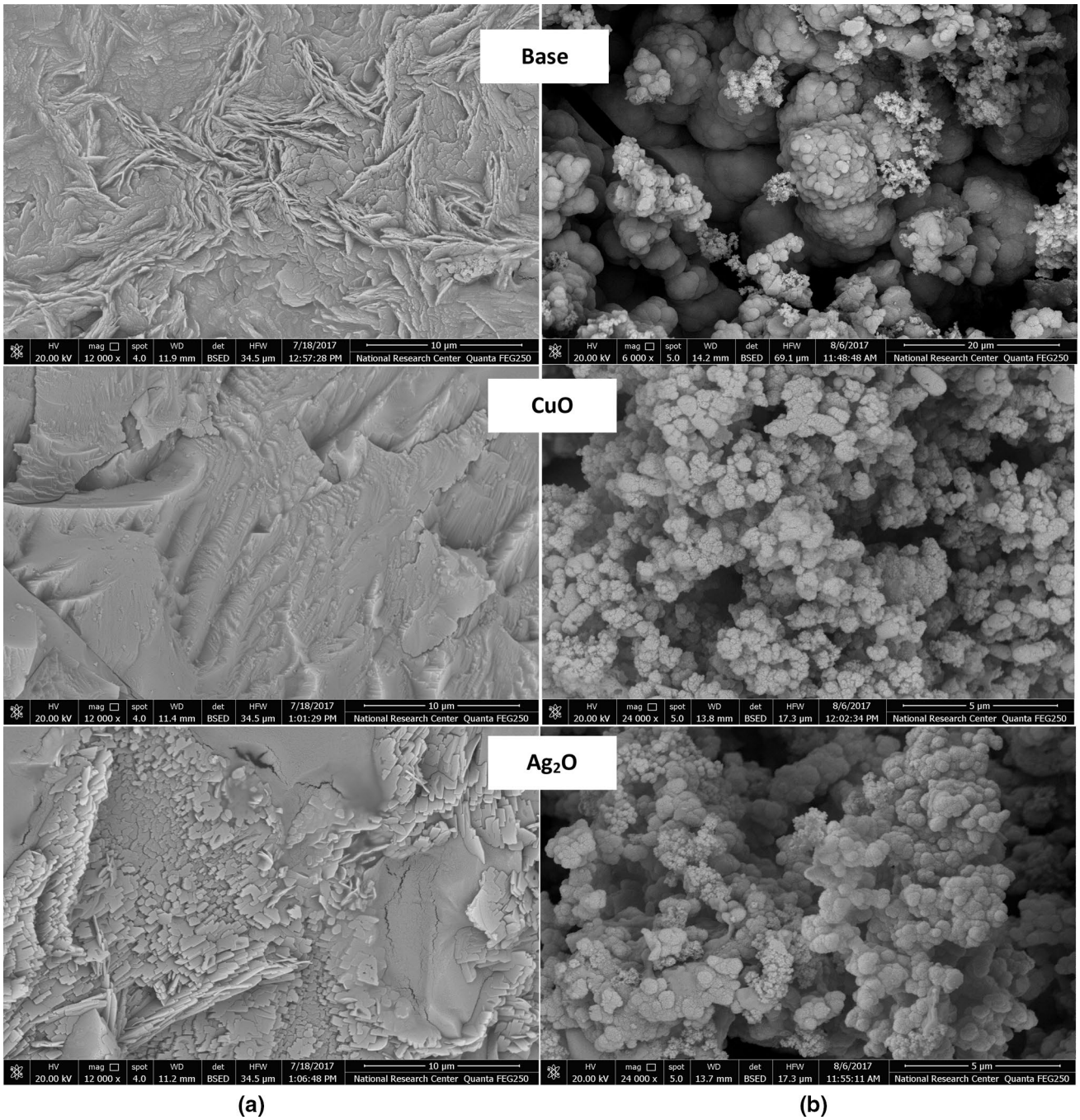

Fig. 7 SEM of the inverted sodium calcium fluorophosphates glass–ceramics **a** before immersion and **b** after immersion

the undoped glass–ceramic, but in the CuO-doped glass–ceramic the nodular structure is covering the most area of the micrograph and the same is evident in the Ag_2O-doped glass–ceramic sample.

Figure 8 illustrates the SEM images of the glass–ceramics of group (2) Na_2O–CaO–P_2O_5 before and after immersion. Careful comparison of Figs. 7 and 8 reveals nearly the same microfeatures or images and the glass–ceramics before immersion exhibit almost the same different shaped microcrystalline features as in Fig. 7. The same nodular-shaped collections or microcrystalline phases are present in the micrograph images of CuO- and Ag_2O-doped glass–ceramics after immersion.

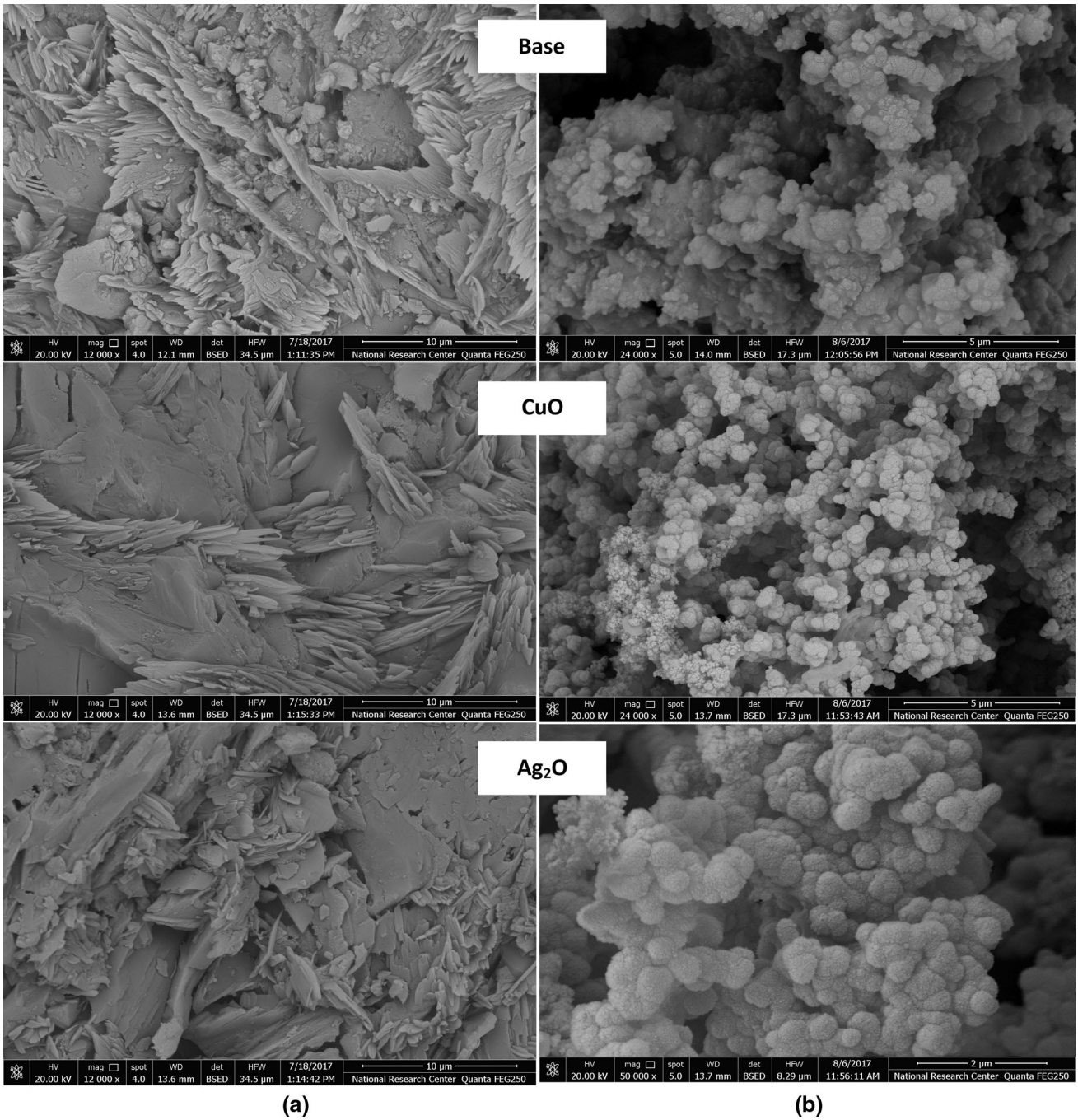

Fig. 8 SEM of the inverted sodium calcium phosphates glass–ceramics **a** before immersion and **b** after immersion

3.4 Optical absorption spectra of the studied glasses

3.4.1 Optical absorption spectra of the $Na_2O–CaF_2–P_2O_5$ glasses

Figure 9a illustrates the optical absorption spectra of the primary undoped glass and that for samples containing 0.2% Ag_2O or 0.2% CuO.

The spectrum of the undoped glass shows strong and wide absorption extending from 200 to about 350 nm with a broad peak centered at about 250 nm without any further absorption up to 1100 nm. The spectrum of the 0.2% Ag_2O-doped sample reveals very close absorption to that of the undoped glass in the UV region, but with lower spectral curve afterward.

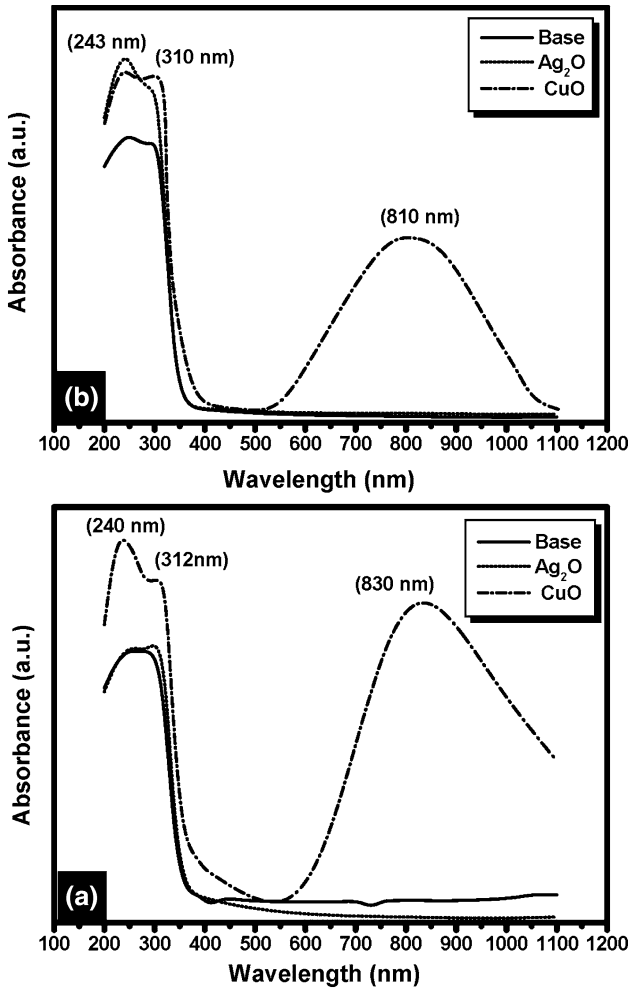

Fig. 9 UV–visible absorption spectra of undoped and Ag_2O or CuO-doped **a** sodium calcium fluorophosphate and **b** sodium calcium phosphate glasses

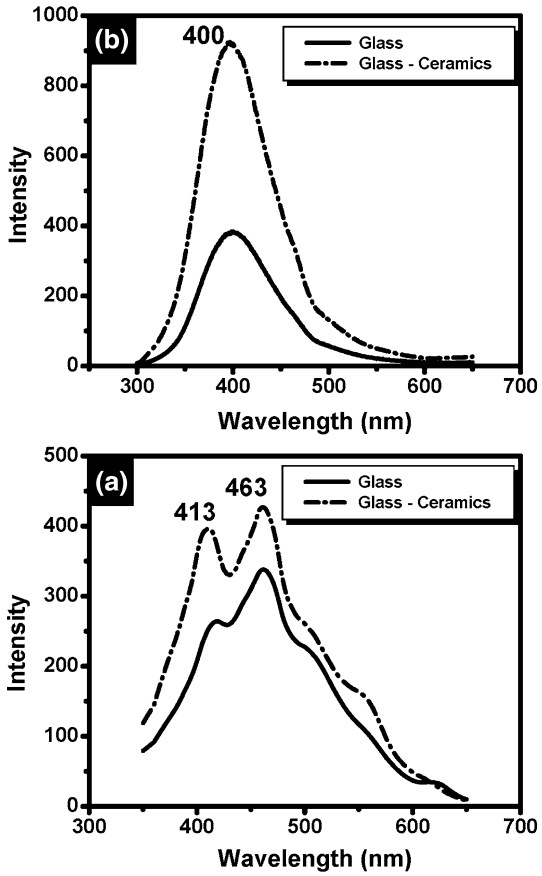

Fig. 10 Photoluminescence spectra of **a** CuO-doped and **b** Ag_2O-doped sodium calcium fluorophosphates glasses and their inverted glass–ceramics

The glass containing 0.2% CuO shows strong UV absorption with higher intensity than that of the undoped sample and with two identified peaks at 240 and 312 nm and followed by a very broad visible–near-IR band extending from about 600 to 1100 nm with a central peak at 830 nm.

3.4.2 Optical absorption spectra of the Na_2O–CaO–P_2O_5 glasses

Figure 9b illustrates the optical spectra of both the primary glass and samples containing 0.2% Ag_2O or 0.2% CuO. The spectrum of the undoped glass consists of strong UV and broad absorption with two peaks at about 250 and 310 nm but with no further identified peaks to the rest of measurement. The Ag_2O-doped glass shows strong UV absorption with higher intensity than that of the undoped glass and revealing a central peak at ~ 250 nm.

The spectrum of the CuO-doped sample reveals higher UV absorption as the Ag_2O-doped sample with two peaks at 243 and 310 nm and with a broad visible–near-IR band extending from 550 to 1100 nm and centered at 810 nm.

3.5 Photoluminescence spectra of the two doped glasses

Figure 10a shows the PL spectra of the CuO-doped glass of the Na_2O–CaF_2–P_2O_5 system and its corresponding glass–ceramic. The glass reveals three connected peaks at 413, 463 and 500 nm, while the glass–ceramic shows two higher intensities peaks at 413 and 463 and two curvatures at the right lobe.

Figure 10b illustrates the PL spectra of the Ag_2O-doped Na_2O–CaF_2–P_2O_5 glass and its glass–ceramic derivative. The spectrum shows a broad band extending from 300 to 600 nm with a peak at 400 nm and the glass–ceramic sample shows a distinctly higher intensity broad band with a peak at 400 nm.

Figure 11a reveals the PL spectra of the CuO-doped $Na_2O–CaO–P_2O_5$ glass and its glass–ceramic derivative. The glass shows four connected peaks at 410, 461, 500 and 550 nm, and the glass–ceramic reveals nearly the same peaks with higher intensity to all the peaks.

Figure 11b illustrates the PL spectra of the Ag_2O-doped $Na_2O–CaO–P_2O_5$ glass and its glass–ceramic derivative. The PL spectrum of the glass shows a very broad band with maximum at 394 nm and the glass–ceramic derivative exhibits a broad band with higher intensity than that of the glass with its peak the same at 394 nm.

4 Discussion

4.1 Interpretation of the X-ray diffraction data

The X-ray diffraction patterns shown in Figs. 1and 2 indicate the separation or formation of three main crystalline phosphate phases, namely two phases of sodium phosphate hydrate and sodium phosphate beside the calcium phosphate crystalline phase and in the case of CaF_2, a fourth phase of sodium calcium fluoride phosphate is identified. The introduction of dopants (CuO or Ag_2O) is observed to change the percent of the three main crystalline phases in addition to a sharing of this dopant as an additional crystalline phase. The previous X-ray data can be interpreted on the following basis:

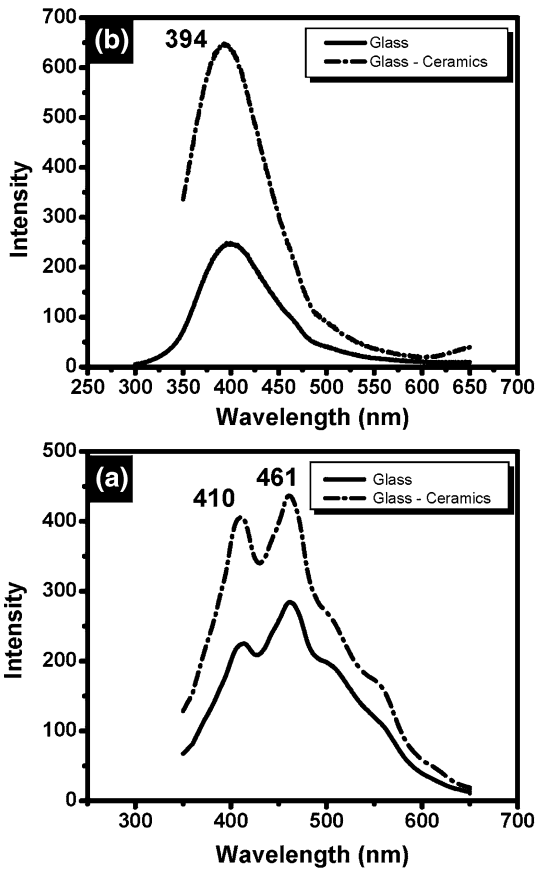

Fig. 11 Photoluminescence spectra of **a** CuO-doped and **b** Ag_2O doped sodium calcium phosphate glasses and their inverted glass–ceramics

(a) It is expected that the type and number of formed crystalline phases upon controlled thermal heat-treatment regime depend on the detailed chemical composition of the base host glass with all its different constituents and on condition of heat treatment [21, 22].

(b) The chemical composition of the base glass contains P_2O_5 (61%) beside Na_2O (27%), CaO (12%) or CaF_2 (12%). These mentioned constituents indicate that the formed crystalline phases are naturally of sodium phosphate and calcium phosphate in accordance with the specific studied chemical composition or even with the formation of mixed sodium calcium fluoride phosphate.

(c) The obvious ease and voluminous crystallization behavior of the base glass can be related to be due to the presence of high percent of phosphorous (P^{5+}) ions and appreciable calcium (Ca^{2+}) ions. McMillan [21] previously assumed that the presence of phosphorous ions even in few percent in glass initiates the formation of phase separation and this situation is highly distinguished for the voluminous and ease of crystallization of Hench's Bioglass being contains 6% P_2O_5 which acts as efficient nucleating agent leading to the formation of soda lime silicate crystalline phases. Hudon and Baker [23] also, reached the conclusion that the presence of Ca^{2+} ions promotes the phase separation and subsequent crystallization of glasses.

4.2 Interpretation of the FTIR spectra of the studied glasses and glass–ceramics

The FTIR spectra shown in Figs. 3 and 4 are interpreted on the following basis [24–28]:

(1) The infrared vibrational bands are expected to depend on the composition of the base host glass which comprises solely of single basic glass-forming units of phosphate groups in accordance with the presence of 61% P_2O_5. This denotes the dual main presence of both Q^2 and Q^3 units of phosphate groups. The vibrational bands are accepted to be finger prints of the structural building phosphate groups of the studied glasses and comparable to similar groups in crystalline analogues.

(2) The distinct far-IR peaks at (400–550) cm^{-1} are related to bending vibrations of O–P–O units, (PO_2) modes of metaphosphate units.
(3) The peak at 711 cm^{-1} can be attributed to symmetric stretching vibrations of the P–O–P linkages.
(4) The peaks within the range 880–1134 cm^{-1} can be related to vibrations due to asymmetric stretching of P–O–P groups.
(5) The peaks within the range 1270–1390 cm^{-1} can be attributed to PO_2 asymmetric stretching of the doubly bonded vibrations (P=O) modes.
(6) The peak at 1457 cm^{-1} can be related to vibrations from many phosphate groups (pyrophosphate) or sharing of vibrations of carbonate groups.
(7) The peak at 1637 cm^{-1} is related to vibrations of OH, water or P–OH bridges.
(8) The near-IR peaks at 2840 and 2927 cm^{-1}, and the broad band centered at 3437 cm^{-1} are correlated with vibrations of water, OH, POH.

4.3 Interpretation of the FTIR spectra after immersion

The examinations of IR spectra after immersion (Figs. 5, 6) and their comparison with similar IR data for the same glasses before immersion (Figs. 3, 4) indicate that the whole IR spectra in Figs. 5 and 6 are obviously simplified and the gathering of multi-vibrational bands is reduced. The most important spectral features of the IR spectra of the glasses and glass–ceramics after immersion are three points:

(1) The persistence of far-IR bands at about (517–550) and (710–735) cm^{-1} with the first band more prominent.
(2) The resolution or the increase in the intensity of the band at about (1113–1150) cm^{-1} to become highly distinctive than the other neighboring mid bands.
(3) The near-IR band around 3425 cm^{-1} becomes constant in intensity of both the glasses and glass–ceramics and for the two varieties of glasses (CaF_2 or CaO).

The previous mentioned changes in the FTIR spectra can be explained as follows:

(a) The simplicity or uniformity of the spectra indicates that the immersion involves uniform corrosion or dissolution processes, which are characteristics for reaction accompanied with ease of dissolution between alkali and alkaline earth phosphate glasses and aqueous solutions [9, 29, 30].
(b) The increase in intensity of the band around 1150 cm^{-1} is related to the appearance of bands which are related to the corrosion process involving the formation of P–OH instead of P–Na or similar groups.
(c) The persistence or appearance of the two far-IR bands at about 550 and 720 cm^{-1} can be correlated with the formation of calcium phosphate during the corrosion or dissolution process, and these two bands are the accepted characteristic bands for hydroxyapatite [8, 9].

4.4 Interpretation of the scanning electron microscopic data

The SEM images shown in Figs. 7 and 8 indicate the appearance of several structural microcrystalline phosphate phases within the textures of the glass–ceramics for the two types of systems containing CaF_2 or CaO. The first group of glass–ceramic reveals numerous small different crystalline phases with various shapes in the base undoped glass–ceramic and with the doped samples, with CuO-doped glass–ceramic uniform texture is identified while with Ag_2O-doped glass–ceramic gathering of small microcrystals are identified. All the glass–ceramics after immersion show rounded or nodular-shaped microcrystals and are more intense in the doped glasses indicating that the dopants CuO and Ag_2O initiate the bioactivity and formation of hydroxyapatite.

The second series of glass–ceramics reveals circular-shaped microcrystals with some grained textures. Also, the glass–ceramic samples after immersion show rounded or nodular-shaped microcrystals which are more identified in the doped samples.

The previous SEM images agree with both the X-ray data and FTIR data after immersion. The different shaped microcrystalline texture of the glass–ceramics before immersion is correlated with the formation of three crystalline phosphate phases with different percents as revealed in the X-ray data. The appearance of rounded or nodular-shaped microcrystals after immersion of the glass–ceramics is in complete agreement with the appearance of the far-IR bands at about 550 and 730 cm^{-1} in the glass–ceramics after immersion, which are known to be characteristic features for the hydroxyapatite formation [8, 9] and hence positive indication of distinctive bioactivity behavior.

4.5 Interpretation of the optical absorption spectra of the studied glasses

The optical spectra shown in Fig. 9 reveal the appearance of strong and broad UV absorption in the two glass

systems either in the undoped base or with both the Ag_2O- and CuO-doped glasses. Such strong UV absorption is attributed to originate from the presence of trace ferric ions which are present contaminated as trace impurity in the chemicals used for the preparation of the studied phosphate glasses. The previous assumption is based on previous derivations by some authors [31, 32] and supported through recent contributions from extended studies by Ehrt [4] and Möncke [5].

The identification of one or two peaks within the UV spectra of the undoped glasses and Ag_2O- and CuO-doped glasses is assumed to be related to the percent of trace ferric impurities. The Ag_2O-doped glasses show no additional absorption bands in the rest of their spectra.

On the other hand, the CuO-doped glasses in the two systems show a very broad visible–near-IR band centered at 810–830 nm. This specific broad band is agreed to be due to the absorption of Cu^{2+} ions in distorted octahedral coordination [33–35]. The broadness and asymmetry of the identified broad band due to divalent copper ions can be assumed to be due to splitting of a low-symmetry ligand field component [34, 35], and Paul [12] assumed that the comparison of the spectra of copper complexes indicated that this broad band is virtually made of up to four overlapping bands which explain the extension of this absorption to wide visible–near-IR region.

4.6 Interpretation of the photoluminescence spectra

Figures 10 and 11 indicate that the PL spectra of CuO-doped glasses of both CaF_2 and CaO types show two main distinct peaks for both the glass and glass–ceramic at (410–413) nm and (461–463) nm. These two visible excitation peaks are assumed by several authors [36, 37] to be related to characteristic PL spectra of Cu^{2+} ions.

This assumption is in conformity of the present optical data which show the appearance of only one broad (visible–near-IR) band which has been attributed to distorted octahedral coordinated Cu^{2+} ions.

There are no distinct variations between the positions of the PL peaks for the two varieties of glasses except minor variations, and the intensities of the glass–ceramic samples are higher than their parent glasses. This may be due to the compact structure with definite crystallographic units in the glass–ceramic derivatives.

The same Figs. 10 and 11 reveal the PL spectra of Ag-doped glasses of both varieties of glasses with an identified peak for the two glasses which occurs at 400 and 394 nm for CaF_2 and CaO, respectively.

The observed single PL peak for both varieties of glasses can be related to be characteristic feature of PL spectra due to the Ag^+ ions present in the glass. The present optical spectra of these two glasses containing Ag_2O did not show any additional UV or visible bands except that UV broad absorption for trace ferric ions present as impurities.

Maurel et al. [38] have identified extra peaks in the spectra of silver zinc phosphate glasses following different irradiations (electron, gamma, laser). Also, the optical spectra did not show the plasmon visible band which is assumed to be of some aggregates or collections of cluster of AgO or any other form as have been cited by some authors [39].

5 Conclusion

Phosphate glasses from the two systems Na_2O–CaO–P_2O_5 and Na_2O–CaF_3–P_2O_5 doped with 0.2% of CuO or Ag_2O were prepared. Their glass–ceramics derivatives were also prepared through two-step regime. Bioactivity behavior of the glasses and glass–ceramics was investigated by FTIR and SEM measurements. The results indicate the appearance of the two far-IR peaks and the rounded or globular-shaped crystalline features which are true indication of the generation of hydroxyapatite giving an indication of bioactivity to the two phosphate systems. X-ray diffraction patterns indicate the formation of various crystalline phosphate phases in accordance with the composition of the parent glass. Additional optical and photoluminescence spectral measurements indicate that these types of fluorophosphates glasses possess optical characteristic to be considered as valuable candidate for optical applications. In conclusion, the fluorophosphates glasses can be recommended to act as both biomaterial and optical candidates.

Compliance with ethical standards

Conflict of interest The authors declare that there is no conflict of interest regarding the publication of this paper.

References

1. Martin W (1991) Review of the structures of phosphate glasses. Eur J Solid State Inorg Chem 28:163–205
2. Brow RK (2000) Review: the structure of simple phosphate glasses. J Non-Cryst Solids 263&264:1–28
3. He Y, Day DE (1992) Development of a low temperature phosphate sealing glass. Glass Technol. 33(6):214–219
4. Ehrt D (2015) Review: phosphate and fluoride phosphate optical glass properties, structure and applications. Phys Chem Glasses Eur J Glass Sci Technol B 56(6):217–234
5. Möncke D (2015) Photo-ionization of 3d-ions in fluoride–phosphate glasses. Int J Appl Glass Sci 6(3):249–267
6. Day DE, Wu Z, Ray CS, Hrma P (1998) Chemically durable iron phosphate glass waste forms. J Non-Cryst Solids 241:1–12
7. Salih V, Franks K, James M, Hastings GW, Knowles JC, Olsen I (2000) Development of soluble glasses for biomedical use

Part II: the biological response of human osteoblast cell lines to phosphate-based soluble glasses. J Mater Sci Mater Med 11(10):615–620
8. Abou Neel EA, Ahmed I, Pratten J, Nazhat SN, Knowles JC (2006) Characterization of antibacterial copper releasing degradable phosphate glass fibres. Biomaterials 26:2247–2254
9. Monem AS, ElBatal HA, Khalil EMA, Azooz MA, Hamdy YM (2008) In vivo behavior of bioactive phosphate glass–ceramics from the system P_2O_5–Na_2O–CaO containing TiO_2. J Mater Sci Mater Med 9:1097–1108
10. Kaur G, Pandey OP, Singh K, Homa D, Scott B, Pickrell G (2014) Review of bioactive glasses: their structure, properties, fabrication and apatite formation. J Biomed Mater Res (A) 102:254–274
11. Franks K, Abrahams I, Georgiou G, Knowles JC (2001) Investigation of thermal parameters and crystallisation in a ternary CaO–Na_2O–P_2O_5-based glass system. Biomaterials 22:497–501
12. Paul A (1990) Chemistry of glasses. Chapman & Hall, NewYork
13. Shelby JE (2005) Introduction to glass science and technology, 2nd edn. The Royal Society of Chemistry, Cambridge
14. Brahmachary K, Rajesh D, Babu S, Ratrakaram YC (2014) Investigations on spectroscopic properties of Pr^{3+} and Nd^{3+} doped zinc-alumino-sodium-phosphate (ZANP) glasses. J Mol Struct 1064:6–14
15. Smith CE, Brow RK (2014) The properties and structure of zinc magnesium phosphate glasses. J Non-Cryst Solids 390:51–58
16. Marzouk MA, Hamdy YM, ElBatal HA (2017) Photoluminescence and spectral performance of manganese ions in zinc phosphate and barium phosphate host glasses. J Non-Cryst Solids 458:1–14
17. Ahmed I, Lewis M, Olsen I, Knowles JC (2004) Phosphate glasses for tissue engineering: part 1. Processing and characterisation of a ternary-based P_2O_5–CaO–Na_2O glass system. Biomaterials 25:491–499
18. Monem AS, ElBatal HA, Khalil EMA, Azooz MA, Hamdy YM (2008) In vivo behavior of bioactive phosphate glass-ceramics from the system P_2O_5–Na_2O–CaO containing TiO_2. J Mater Sci Mater Med 16:1097–1108
19. Ahmed AA, Ali AA, Mahmoud DAR, El-Fiqi AM (2011) Study on the preparation and properties of silver-doped phosphate antibacterial glasses (Part I). Solid State Sci 13:981–992
20. Kokubo T, Kushitani H, Sakka S, Kitsugi T, Yamamuro T (1990) Solutions able to reproduce in vivo surface-structure changes in bioactive glass–ceramic A-W^3. J Biomed Mater Res (A) 24:721–734
21. McMillan PW (1979) Glass-ceramics, 2nd edn. Academic Press, London
22. Holland W, Beall G (2002) Glass-ceramic technology. The American Ceramic Society, Westerville
23. Hudon P, Baker DR (2002) The nature of phase separation in binary oxide melts and glasses. J Non-Cryst Solids 303(3): 299–345, 346–353
24. ElBatal FH (2008) Gamma ray interaction with copper-doped sodium phosphate glasses. J Mater Sci 43:1070–1079
25. Znáši P, Jamnický M (1992) Preparation, infrared spectra, and structure of glasses in the system CuCl–Cu_2O–(P_2O_5 + MoO_3). J Non-Cryst Solids 146:74–80
26. Moustafa YM, El-Egili K (1998) Infrared spectra of sodium phosphate glasses. J Non-Cryst Solids 240:144–153
27. Chahine A, El-Tabirou M, El-Benaissi M, Haddad M, Pascal JL (2004) Effect of CuO on the structure and properties of (50 − *x*/2) Na_2O-*x*CuO-(50 − *x*/2)P_2O_5 glasses. Mater Chem Phys 84:341–347
28. Marzouk MA, Fayad AM, ElBatal HA (2017) Correlation between luminescence and crystallization characteristics of Dy^{3+} doped P_2O_5–BaO–SeO_2 glasses for white LED applications. J Mater Sci Mater Electron 28:13101–13111
29. Bunker B, Arnold G, Wilder JA (1984) Phosphate glass dissolution in aqueous solutions. J Non-Cryst Solids 64(3):291–316
30. Gao H, Tan T, Wang D (2004) Dissolution mechanism and release kinetics of phosphate controlled release glasses in aqueous medium. J Control Release 96(1):29–36
31. Sigel GH Jr. (1977) Optical absorption of glasses. In: Tomozawa M, Doremus RH (eds) Treatise in materials science and technology, vol 12. Academic Press, SanDiego, pp 5–89
32. Cook L, Mader KH (1982) Ultraviolet transmission characteristics of a fluorophosphate laser glass. J Am Ceram Soc 65:597–601
33. Metwalli E (2003) Copper redox behavior, structure and properties of copper lead borate glasses. J Non-Cryst Solids 317:221–230
34. Duran A, Navarro JMF (1985) The colouring of glass by Cu^{2+} ions. Phys Chem Glasses 26:126–131
35. Murali Krishna C, AnilaKumari B, Reddy MS, Veeraiah N (2007) Characterization and physical properties of Li_2O–CaF_2–P_2O_5 glass ceramics with Cr_2O_3 as a nucleating agent—physical properties. J Solid State Chem 180:2747–2755
36. Sudhakar Reddy B, Buddhudu S (2007) Spectral analysis of Cu^{2+} and Mn^{2+} ions doped borofluorophosphate glasses. Bull Mater Sci 30(5):481–486
37. Pal I, Agarwal A, Sanghi S (2012) Spectral analysis and structure of Cu^{2+}-doped cadmium bismuth borate glass. Indian J Pure Appl Phys 50(4):237–244
38. Maurel C, Cardinal T, Bellec M, Canioni L, Bousquet B, Treguer M, Videau JJ, Choi J, Richardson M (2009) Luminescence properties of silver zinc phosphate glasses following different irradiations. J Lumin 129:1514–1518
39. Abdelghany AM, ElBatal HH, ElBatal FH (2015) Spectral studies of silver ions in barium borate glass and effects of gamma irradiation. Middle East J Appl Sci 5(5):7–17